Int. J. Multiphase Flow Vol. 14, No. 2, pp. 189–202, 1988
Printed in Great Britain.

0301-9322/88 $3.00 + 0.00

TRANSIENT DROPLET EVAPORATION WITH VARIABLE PROPERTIES AND INTERNAL CIRCULATION AT INTERMEDIATE REYNOLDS NUMBERS

M. RENKSIZBULUT and R. J. HAYWOOD
Mechanical Engineering Department, University of Waterloo, Waterloo, Ontario N2L 3G1, Canada

(*Received* 13 *August* 1986; *in revised form* 13 *November* 1987)

Abstract—The energetics and dynamics of *n*-heptane droplets evaporating in their own 800 K vapour at 1 and 10 bar have been studied using a finite-volume-based numerical method at intermediate Reynolds numbers. Droplet mass, Reynolds number, liquid heating rate, Nusselt number and drag coefficient histories have been obtained. The results show that liquid-phase heating plays an important role in overall droplet behaviour, particularly at elevated pressures. A simple liquid heating model is also presented which accounts for internal circulation through the use of an effective thermal conductivity. This enhanced diffusion model, together with a set of heat transfer and drag correlations, is shown to predict droplet behaviour in good agreement with the detailed numerical results.

1. INTRODUCTION

Liquid sprays are extensively used in a variety of devices ranging from simple fire sprinklers to complex propulsion systems. This has naturally led to much interest in the study of droplet evaporation and combustion processes. In a comprehensive review paper on spray evaporation and combustion, Faeth (1983) identified a number of separated flow models which are capable of predicting the behaviour of practical sprays. Due to computational limitations, such models make no attempt to calculate the details of the flow around individual droplets, but rather employ a Lagrangian formulation to track the motion of the droplets in the spray field which requires correlations for droplet drag and, heat and mass transfer. Clearly, a complete understanding of droplet energetics and dynamics is fundamental to this important class of spray modelling and to the understanding of liquid sprays in general.

Droplet processes that take place in a typical spray environment are diverse and complex to model. Following the primary atomization of the liquid jet and the subsequent break-up of larger droplets, a spectrum of drop sizes and velocities is established. Droplet trajectories depend on the injector type and system characteristics. However, in general, smaller droplets with diameters less than about 20 μm which possess little inertia readily conform to the local flow structure. For these droplets, the associated Reynolds numbers are close to zero over most of their lifetimes, and comprehensive literature reviews by Williams (1973), Faeth (1977, 1983), Law (1983) and Sirignano (1983) suggest that the behaviour of such droplets is reasonably well-understood within the framework of the classical spherically-symmetric analyses pioneered by Godsave (1953) and Spalding (1953). On the other hand, larger droplets with typical diameters of the order of 70–80 μm possess sufficient inertia to penetrate deep into the spray region with essentially straight trajectories. For these larger droplets, convective transport processes remain dominant throughout the droplet lifetime which is typically spent in the so-called intermediate Reynolds number range (from about 5 to 500), where neither the creeping-flow nor the boundary-layer type of analyses may rigorously be applied. It is the behaviour of such large droplets that the present work is concerned with.

The evaporation process itself brings about two major changes in the flow field around a sphere. Firstly, the composition of the gas phase is modified—which in most cases results in very significant changes in the thermophysical properties, and therefore, in the associated heat, mass and momentum transfer rates. Secondly, the evaporation process produces an effect similar to non-uniform blowing at the surface—which retards heat transfer to the droplet, reduces friction drag and increases pressure drag. The problem is further complicated by liquid-phase heating and motion.

2. LITERATURE REVIEW

Readers interested in the low Reynolds number behaviour of evaporating droplets will find the papers by Taylor & Acrivos (1964), Fendell *et al.* (1966), Gal-Or & Yaron (1973), Montlucon (1975), Sadhal & Ayyaswamy (1983) and Gogos *et al.* (1986) extremely useful. The present work is concerned with the behaviour of larger droplets, and therefore, the literature review here will be confined to studies carried out in the intermediate Reynolds number range.

The inherently transient, convective, two-phase and multicomponent nature of the droplet evaporation process has rendered its quantitative analysis quite difficult, even under idealized conditions. Prakash & Sirignano (1980) used an integral boundary-layer formulation together with the assumption of a quasi-steady gas phase. Their analysis included limited variable property effects, and processes due to liquid-phase circulation and transient heating. The results showed that liquid heating persists throughout the droplet lifetime and therefore plays an important role in the overall evaporation process. The model was later extended to the analysis of multicomponent droplet evaporation by Lara-Urbaneja & Sirignano (1981). Although this approach captures much of the relevant physics, it is not entirely satisfactory for several reasons. Firstly, at the Reynolds numbers of interest ($\mathrm{Re} \simeq 100$), the boundary-layer assumptions are not very satisfactory and obviously, completely break down beyond the point of flow separation. Secondly, the imposition of the potential flow pressure distribution on the boundary layer makes the all important determination of the droplet drag coefficient impossible. Finally, the strongly coupled and highly non-linear nature of the governing equations make recourse to numerical methods inevitable and therefore, the benefits of such a semi-analytical approach over a completely numerical one are questionable.

Using the stream-function/vorticity formulation and a non-orthogonal adaptive grid to track the shrinking droplet, Dwyer & Sanders (1984a, b) numerically solved the transient transport equations for both the liquid and gas phases. Unfortunately, in these studies the effects of variable thermophysical properties were ignored. Considering the fact that very large temperature and concentration gradients typically exist in the transfer paths, the assumption of constant properties is a major limitation which makes the interpretation of the results difficult and somewhat ambiguous.

Renksizbulut & Yuen (1983a) also used numerical methods to analyse the behaviour of evaporating droplets in high-temperature convective surroundings. Although the evaporation process was treated as quasi-steady, and the effects of liquid motion and heating were ignored, all effects due to variable thermophysical properties were considered. This study, concurrently carried out with an experimental investigation (Renksizbulut & Yuen 1983b) of droplet evaporation in air streams up to 1059 K, resulted in the following correlations:

—droplet drag ($10 < \mathrm{Re}_m < 300$),

$$C_D(1 + B_f)^{0.2} = 24\,\mathrm{Re}_m^{-1} + 4.8\,\mathrm{Re}_m^{-0.37}; \qquad [1]$$

—heat transfer ($10 < \mathrm{Re}_m < 2000$),

$$\mathrm{Nu}_f(1 + B_f)^{0.7} = 2 + 0.57\,\mathrm{Re}_m^{1/2}\,\mathrm{Pr}_f^{1/3}; \qquad [2]$$

where C_D is the drag coefficient, and Re, Pr, Nu and B are the Reynolds, Prandtl, Nusselt and transfer numbers, respectively. Complete definitions of all dimensional and non-dimensional variables are given in the nomenclature section. In both equations, all thermophysical properties are evaluated using the film conditions (arithmetic average molar concentration and temperature), except for density in Re_m which is based on the free-stream value. The r.h.s.s of [1] and [2] are recognizable as standard forms for flow over solid spheres at intermediate Reynolds numbers. The terms $(1 + B_f)^{0.2}$ and $(1 + B_f)^{0.7}$ account for the reductions in total drag and heat transfer due to the blowing effect of evaporation, as characterized by the transfer (or Spalding) number B. Renksizbulut & Yuen (1983a, b) have demonstrated that these correlations predict well the experimental and numerical data of other researchers using different fluids as well as data on solid spheres ($B = 0$).

Recently, Haywood & Renksizbulut (1986) carried out a more detailed numerical study in order to examine the predictive capabilities of [1] and [2]. The life history of an n-heptane droplet introduced to an environment of its own vapour at 1 bar, 800 K, with an initial Reynolds number of 100 was studied. All effects due to variable properties, liquid-phase motion and heating, and transient variations in droplet size and velocity were included in the analysis. The choice of an all heptane gas phase ensured a very accurate assessment of the effects of variable properties by removing the inherent uncertainties associated with the prediction of multicomponent gas properties. The results showed, as expected, that liquid-phase heating plays an important role, and that [1] and [2] will predict the droplet drag and heat transfer rates accurately only when liquid-phase heating is accounted for through the use of an effective latent heat of vaporization L' in the calculation of the transfer number. L' is simply defined from the surface energy balance:

$$Q_G^* = \dot{m}^* L^* + Q_L^* \equiv \dot{m}^* L^{*\prime}, \qquad [3]$$

where $\dot{m}$ is the rate of evaporation and * designates a dimensional variable. Clearly, a practical model is needed for the prediction of heat transfer to the liquid phase, Q_L^*, if these correlations are to be of value in spray modelling studies. This constitutes one of the major objectives of the present work.

3. PROBLEM STATEMENT AND ASSUMPTIONS

Life histories of n-heptane droplets evaporating in superheated n-heptane streams at 800 K at 1 and 10 bar, are traced. The initial Reynolds numbers have been selected as 100 and 250 for the 1 and 10 bar cases, respectively. In both cases, the liquid-phase temperature is initially 298 K, which is well below the boiling point temperatures of 372 K at 1 bar and 478 K at 10 bar.

It is assumed that the droplet maintains a perfectly spherical shape at all times, the flow field is laminar and axisymmetric, and all effects due to gravity, viscous dissipation and thermal radiation are negligible. It is further assumed that thermodynamic equilibrium exists at the gas–liquid interface and therefore, the droplet surface is at the boiling point at all times. The flow conditions existing inside and outside the droplet at the time of formation cannot be described with any degree of certainty. In view of this, the initial flow field has been arbitrarily prescribed as isothermal viscous flow over a motionless liquid sphere at the specified initial Reynolds number.

4. THE FULLY NUMERICAL MODEL

Based on the non-dimensionalization given in the nomenclature section, the transport equations expressing the conservation of mass, momentum and energy can be cast into the following unified format:

$$\frac{\partial}{\partial t}(\rho V R \Phi) + V^2 \nabla \cdot \left\{ \rho \Phi \left[\left(v_r - \frac{r}{V}\frac{\mathrm{d}R}{\mathrm{d}t} \right) \hat{r} + v_\theta \hat{\theta} \right] \right\} = \frac{V}{R} \nabla \cdot (\Gamma_\Phi \nabla \Phi) + S_\Phi. \qquad [4]$$

Where:

for the continuity equation, $\Phi = 1$, $\Gamma_C = 0$ and

$$S_C = \rho R \frac{\mathrm{d}V}{\mathrm{d}t} - 2\rho V \frac{\mathrm{d}R}{\mathrm{d}t}; \qquad [5]$$

for the radial momentum, $\Phi = v_r$, $\Gamma_{RM} = 2\mu/\mathrm{Re}_0$ and

$$S_{RM} = V^2[\nabla \cdot (\rho \mathbf{v} v_r) - \nabla \cdot (\rho \mathbf{v}\mathbf{v})_r] - \frac{2V}{\mathrm{Re}_0 R}[\nabla \cdot \mu \nabla v_r - (\nabla \cdot \tau)_r] - 2\rho V v_r \frac{\mathrm{d}R}{\mathrm{d}t} - \frac{\partial p}{\mathrm{d}r}; \qquad [6]$$

for the tangential momentum equation $\Phi = v_\theta$, $\Gamma_{TM} = 2\mu/\mathrm{Re}_0$ and

$$S_{TM} = V^2[\nabla \cdot (\rho \mathbf{v} v_\theta) - \nabla \cdot (\rho \mathbf{v}\mathbf{v})_\theta] - \frac{2V}{\mathrm{Re}_0 R}[\nabla \cdot \mu \nabla v_\theta - (\nabla \cdot \tau)_\theta] - 2\rho V v_\theta \frac{\mathrm{d}R}{\mathrm{d}t} - \frac{1}{r}\frac{\partial p}{\partial \theta}; \qquad [7]$$

finally, for the energy equation, $\Phi = T$, $\Gamma_E = 2k/(c_p \mathrm{Re}_0 \mathrm{Pr}_\infty)$ and

$$S_E = \rho T R \frac{dV}{dt} - 2\rho T V \frac{dR}{dt} + \frac{2V}{\mathrm{Re}_0 \mathrm{Pr}_\infty R} \frac{k}{c_p^2} (\nabla T \cdot \nabla c_p). \quad [8]$$

These equations were solved subject to the following set of boundary conditions in the solution domain shown in figure 1.

(a) At the droplet surface, $r = 1$:

$$T_s = T_{sat}, \quad [9]$$

$$\tau_{r\theta,G} = \tau_{r\theta,L}, \quad v_{\theta,G} = v_{\theta,L}, \quad [10]$$

$$v_{r,L} = \frac{1}{V}\left(\frac{\dot{m}''_\theta}{\rho_L} + \frac{dR}{dt}\right), \quad [11]$$

$$v_{r,G} = \frac{1}{V}\left(\frac{\dot{m}''_\theta}{\rho_G} + \frac{dR}{dt}\right), \quad [12]$$

$$-k \left.\frac{\partial T}{\partial r}\right|_L = -k \left.\frac{\partial T}{\partial r}\right|_G + \tfrac{1}{2}\mathrm{Re}_0 \mathrm{Pr}_\infty R \dot{m}''_\theta L; \quad [13]$$

where the stress component $\tau_{r\theta}$ is given by

$$\tau_{r\theta} = \mu r \frac{\partial}{\partial r}\left(\frac{v_\theta}{r}\right) + \frac{\mu}{r}\frac{\partial v_r}{\partial \theta}. \quad [14]$$

(b) Far from the droplet, $r = 40$ and $0 \leqslant \theta \leqslant \pi/2$:

$$v_r = -\cos\theta, \quad v_\theta = \sin\theta, \quad T = 1. \quad [15]$$

(c) Far from the droplet, $r = 40$ and $\pi/2 < \theta \leqslant \pi$:

$$\frac{\partial \xi}{\partial r} = 0, \qquad \text{where } \xi = v_r,\ v_\theta,\ T. \quad [16]$$

(d) Along the axis of symmetry, $v_\theta = 0$ and:

$$\frac{\partial \xi}{\partial \theta} = 0, \qquad \text{where } \xi = v_r,\ T. \quad [17]$$

Equation [16] presents an adequate solution to the well-known problem of specifying downstream boundary conditions at a finite distance from an object in computational fluid mechanics and heat transfer.

Overall conservation of mass and momentum provides the expressions necessary to close the equation set:

$$\frac{dR}{dt} = -\frac{1}{2\bar{\rho}_L}\int_0^\pi \dot{m}''_\theta \sin\theta \, d\theta - \frac{R}{3\bar{\rho}_L}\frac{d\bar{\rho}_L}{dt} \quad [18]$$

and

$$\frac{dV}{dt} = -\frac{3C_D V^2}{8\bar{\rho}_L R}. \quad [19]$$

The total drag coefficient C_D is the sum of the friction drag C_F, pressure drag C_P and the thrust C_T coefficients which are calculated at the droplet surface, based on the instantaneous gas flow field using

$$C_F = \left(\frac{8}{RV\mathrm{Re}_0}\right)\int_0^\pi (\tau_{r\theta}\sin\theta - \tau_{rr}\cos\theta)\sin\theta \, d\theta, \quad [20]$$

$$C_P = \int_0^\pi \left(\frac{2p}{V^2}\right)\sin 2\theta \, d\theta \quad [21]$$

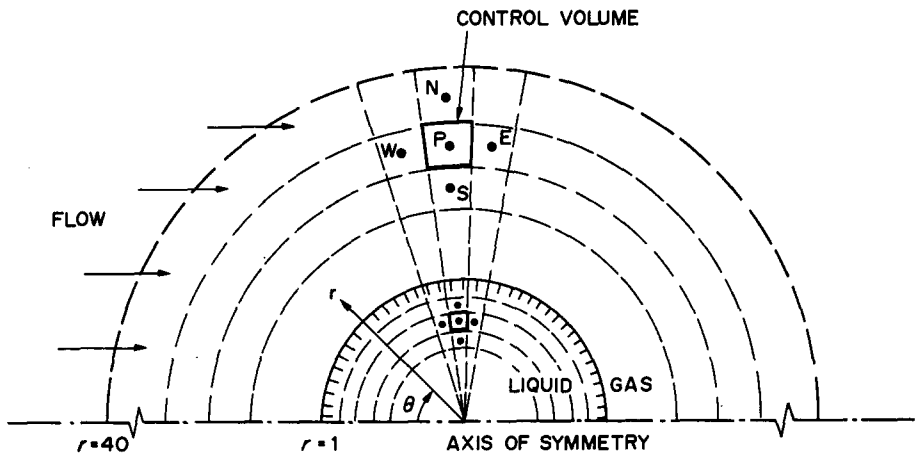

Figure 1. The numerical solution domain and grid layout.

and

$$C_T = \int_0^{\pi} 2\rho v_r^2 \sin 2\theta \, d\theta - \int_0^{\pi} 4\rho v_r v_\theta \sin^2 \theta \, d\theta, \quad [22]$$

where the stress component τ_{rr} is given by

$$\tau_{rr} = 2\mu \frac{\partial v_r}{\partial r} - \frac{2}{3}\mu \nabla \cdot \mathbf{v}. \quad [23]$$

In order to solve the above set of non-linear and strongly coupled equations, a conservative finite-volume-based numerical technique was used. The governing differential equations were integrated over discrete volumes, sketched in figure 1, resulting in a set of algebraic equations of the generalized form

$$A_P \Phi_P = A_N \Phi_N + A_S \Phi_S + A_E \Phi_E + A_W \Phi_W + B_P, \quad [24]$$

which were solved iteratively using the ADI (alternating direction implicit) technique. The lengthy derivation which leads to [24] and the coefficient functions A_P, A_N, A_S, A_E, A_W and B_P are given by Haywood (1986). In working numerically with the so-called primitive variables (v_r, v_θ, p), the absence of an explicit equation for pressure presents a problem. In the present work, this difficulty was overcome by using the SIMPLEC approach (Patankar 1980; Vandoormaal & Raithby 1984), in which an expression in the form of [24] was derived for pressure by a combination of the continuity and momentum equations. The basic strategy is to develop a pressure field such that the resulting velocity field satisfies the continuity equation for every control volume in the calculation domain. Further details of the entire numerical procedure and the verification of the computer code through benchmark problems are given by Haywood (1986).

5. RESULTS OF THE FULLY NUMERICAL MODEL

As indicated in section 3, two cases were studied. The first case which involved the evaporation of an n-heptane droplet at 1 bar has been discussed in detail previously (Haywood & Renksizbulut 1986) and will not be repeated here. However, some of the results have been reproduced in figures 2–4 in order to point out some of the earlier observations and to provide a comparison basis for the second case involving droplet evaporation at 10 bar.

Figure 2 shows that over 80% of the droplet lifetime is spent at $Re > 10$, and that liquid-phase heating persists for a period covering about one-third of the droplet lifetime. The effect of liquid heating on overall droplet behaviour is apparent in figures 3 and 4, where the average Nusselt number is calculated based on the instantaneous gas-phase temperature field using

$$Nu_\infty = \frac{1}{(1 - T_s)} \int_0^{\pi} \left(k \frac{\partial T}{\partial r} \right)_s \sin \theta \, d\theta. \quad [25]$$

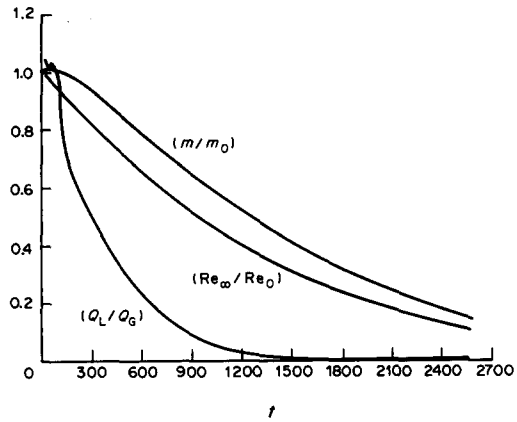

Figure 2. Liquid heating fraction, droplet mass and Reynolds number histories at 1 bar; $Re_0 = 100$.

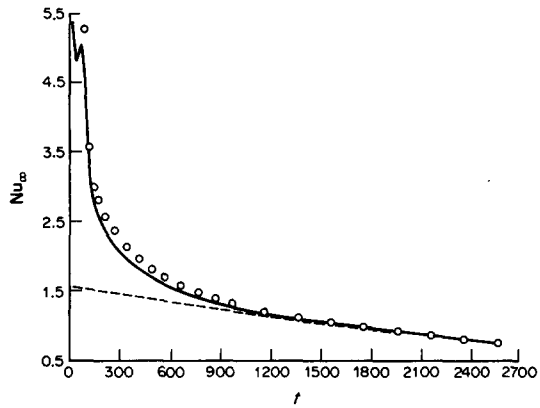

Figure 3. Nusselt number history at 1 bar ($Re_0 = 100$): ○, fully numerical solution; ----, [2]; ——, [2] with B' as defined by [26].

It is seen that the unmodified Renksizbulut–Yuen correlations as given by [1] and [2] can be used in a quasi-steady manner to obtain excellent predictions, but only beyond the period of appreciable liquid heating. This is not surprising because, in general, gas-phase heat and momentum diffusion rates (as characterized by α_G and ν_G) at atmospheric pressure are 2–3 orders of magnitude larger than typical droplet surface regression rates (as characterized by dR^2/dt), whereas even with internal circulation, transport rates in the liquid phase are comparable in magnitude to dR^2/dt. Clearly, a quasi-steady treatment is readily justifiable in the absence of significant liquid heating. However, as shown in figures 3 and 4, transient effects due to liquid heating can still be handled in a quasi-steady manner provided that the correlations are modified by using an effective latent heat of vaporization L' (defined by [3]) in the transfer number definition, such that

$$B_f' = (T_\infty^* - T_s^*)c_{p,G,f}^*/L^{*\prime}. \qquad [26]$$

In the 10 bar case, the initial Reynolds number was chosen to be $Re_0 = 250$ corresponding, for example, to a 50 μm dia droplet with an initial relative velocity of about 5 m/s. In view of the higher gas density and droplet surface temperature (lower surface tension), such a droplet may be initially somewhat deformed. Droplets are nearly spherical when $We \ll 10$ (Williams 1985). For the example given above, the initial $We < 5$ (which corresponds to the worst conditions), indicating that the assumption of a spherical droplet is still a realistic one.

The droplet mass, liquid heating fraction and Reynolds number histories for the 10 bar case are shown in figure 5. As expected, at this pressure level the droplet lifetime is found to be much

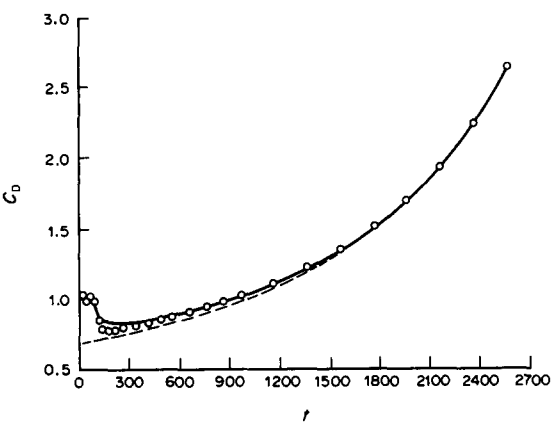

Figure 4. Total drag coefficient history at 1 bar ($Re_0 = 100$): ○, fully numerical solution; ----, [1]; ——, [1] with B' as defined by [26].

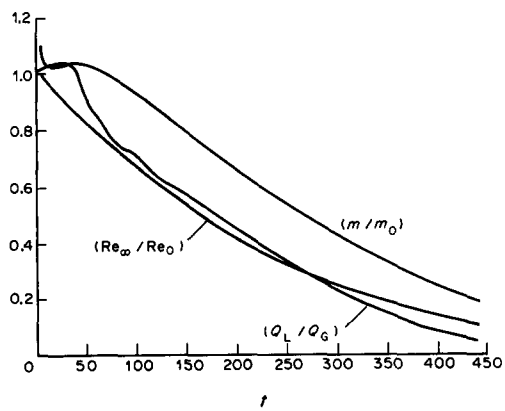

Figure 5. Liquid heating fraction, droplet mass and Reynolds number histories at 10 bar; $Re_0 = 250$.

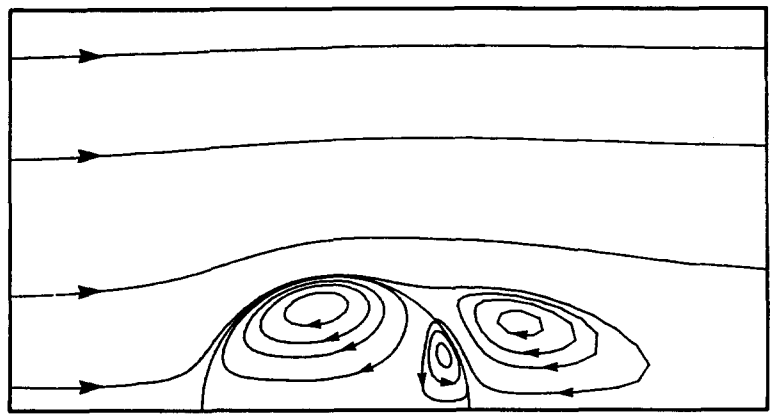

Figure 6. The flow field early in the droplet lifetime during the condensation period; $p = 10$ bar, $\mathrm{Re}_\infty = 243$, $t = 10$.

shorter, predominantly due to the 10-fold increase in the gas-phase density, resulting in enhanced convective transport. Similarly to the 1 bar case, about 80% of the droplet lifetime is spent at $\mathrm{Re} > 0.1\ \mathrm{Re}_0$. The initial increase in droplet mass that is observed in this figure and also in figure 2, is due to vapour condensation on the subcooled droplet. With a prescribed initial subcooling of $T_s - T_0 = 180$ K compared to 74 K in the low-pressure case, the condensation period is now substantially longer as a fraction of the droplet lifetime.

Figure 5 also shows that at 10 bar liquid-phase heating persists for almost the entire droplet lifetime. There are a number of competing effects brought about by increased pressure which alter the duration and intensity of liquid-phase heating, thereby influencing overall droplet behaviour. At elevated pressures, increased gas density and reduced liquid viscosity (due to higher droplet temperatures) both act to intensify liquid-phase motion. The complexity of the resulting flow fields is self-evident in figures 6 and 7. Figure 6 shows the existence of even a secondary recirculation zone in the liquid phase driven by the strong flow reversal of the gas-phase trailing vortex. However, this secondary recirculation zone dies out very quickly and has a negligible effect on heat transfer.

Present numerical results show the maximum tangential velocity at the droplet surface attaining 24% of the corresponding gas-phase free-stream velocity, v_∞, early in the droplet lifetime and then decaying to $0.10v_\infty$ towards the end, both of which are much larger than $0.09v_\infty$ and $0.03v_\infty$, respectively, encountered in the low-pressure case (Haywood & Renksizbulut 1986). Intensified internal circulation alone would lead one to believe that liquid-phase heating time should be shorter. However, at elevated pressures, three other effects compete with this. Firstly, the saturation

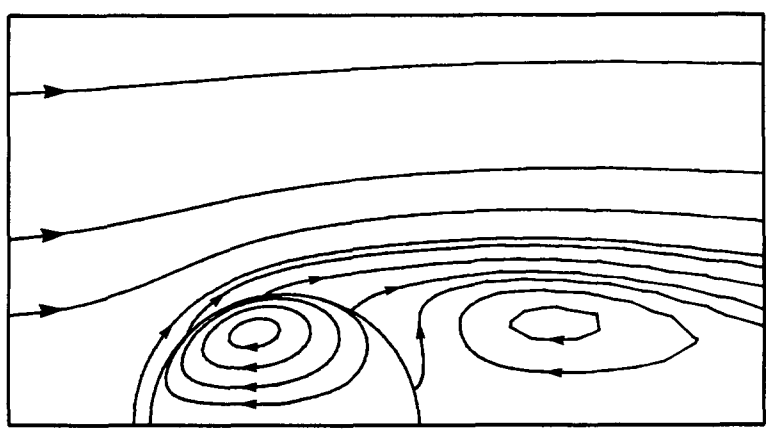

Figure 7. The flow field during the evaporation period; $p = 10$ bar, $\mathrm{Re}_\infty = 76$, $t = 261$.

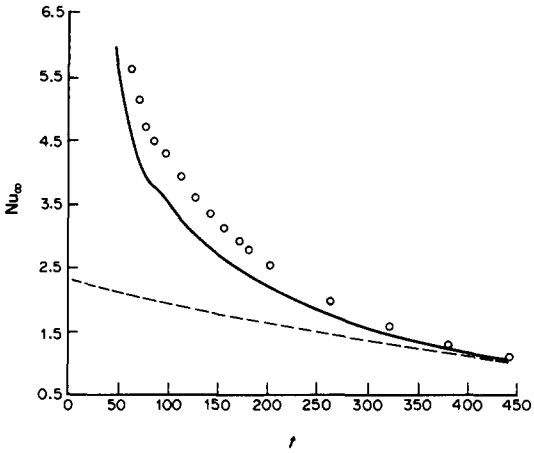

Figure 8. Nusselt number history at 10 bar ($Re_0 = 250$): ○, fully numerical solution; ----, [2]; ——, [2] with B' as defined by [26].

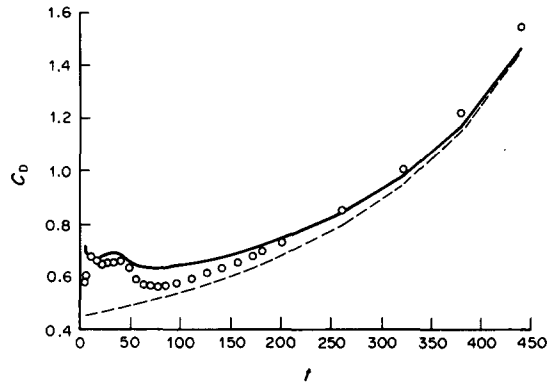

Figure 9. Total drag coefficient history at 10 bar ($Re_0 = 250$): ○, fully numerical solution; ----, [1]; ——, [1] with B' as defined by [26].

temperature is higher which normally results in a higher degree of initial liquid subcooling. Secondly, because of higher droplet temperatures, liquid thermal conductivity is substantially reduced. For example, k_L at 478 K (T_s at 10 bar) is less than 65% of its value at 371 K (T_s at 1 bar). Thirdly, at elevated pressures, the surface regression rate is higher. Consider the limiting situation where the surface regresses as fast as the thermal wave propagates in the liquid phase. This would result in a time-invariant interface temperature gradient and therefore, liquid heating would persist for the entire droplet lifetime. Hence, these three effects override the thermal benefits of enhanced internal circulation and prolong liquid heating times at elevated pressures.

Figures 8 and 9 show the computed Nusselt number and drag histories as well as the predicted values using the Renksizbulut–Yuen correlations in a quasi-steady manner with and without correction for liquid heating. Compared to the low-pressure case (see figures 3 and 4) the agreement is not as good because of increased liquid surface mobility and the deterioration of gas-phase quasi-steadiness with increasing pressure. The former follows from the fact that the r.h.s.s of [1] and [2] represent solid sphere-like conditions, and therefore, both correlations fail to some extent when there is a great deal of liquid-phase motion present. The latter is apparent, for example, from the ratio of the gas-phase thermal diffusion rate to the surface regression rate:

$$\frac{\alpha_G^*}{\dfrac{dR^{*2}}{dt^*}} = \left(Re_0 Pr_\infty R \frac{dR}{dt}\right)^{-1}. \qquad [27]$$

With $Re_0 \simeq 100$, $Pr_\infty \simeq 1$, $R \simeq 1$ and $dR/dt \simeq 10^{-3}$, this ratio is only of order 10, which is clearly quite marginal for a quasi-steady treatment. Nevertheless, the predictive capabilities of the correlations are quite remarkable in view of the complexity of the problem.

6. THE SEMI-ANALYTICAL MODEL

Although the complete numerical model provides detailed information on the flow field and the transport processes taking place during droplet evaporation, its complexity and cost renders it rather useless for spray modelling. Motivated by this, a much simpler semi-analytical model was formulated. The overall conservation of mass, momentum and energy can be expressed in the form:

$$\frac{dm^*}{dt^*} = -\dot{m}^*, \qquad [28]$$

$$m^* \frac{dv_\infty^*}{dt^*} = -\tfrac{1}{2}\rho_\infty^* v_\infty^{*2} \pi R^{*2} C_D \qquad [29]$$

and

$$\dot{m}^* L^{*\prime} = Q_G^* = 4\pi R^{*2} h^* (T_\infty^* - T_s^*), \quad [30]$$

where $m^* = (4/3)\pi R^{*3} \rho_L^*$, h^* is the heat transfer coefficient and $L^{*\prime}$ is defined by [3] as

$$L^{*\prime} = \frac{L^*}{\left(1 - \frac{Q_L^*}{Q_G^*}\right)} \quad [31]$$

Hence, if a simple method for calculating the liquid-phase heating rate Q_L^* (or Q_L^*/Q_G^*) can be found, then with appropriate heat transfer and drag correlations, and a given set of initial conditions, these equations can be easily solved using basic numerical integration techniques.

The present liquid heating model is basically an enhanced diffusion model. The starting point is the well-known analytical solution for transient, one-dimensional conduction inside a sphere with prescribed initial and surface temperatures (Carslaw & Jager 1959) which yields the following expression for the temperature gradient at the surface of the sphere:

$$\left[\frac{\partial T^*}{\partial r^*}\right]_s = \frac{2(T_s^* - T_0^*)}{R^*} \sum_{j=1}^{\infty} \exp\left(\frac{-j^2 \pi^2 k_L^* t^*}{\rho_L^* c_{p,L}^* R^{*2}}\right). \quad [32]$$

The liquid heating fraction is then calculated from

$$\frac{Q_L^*}{Q_G^*} = \frac{k_L^* \left(\frac{\partial T^*}{\partial r^*}\right)_s}{h^*(T_\infty^* - T_s^*)}. \quad [33]$$

Clearly, [32] is not readily applicable to the case of an evaporating droplet with surface regression and internal circulation. The effects of surface regression can be modelled by using a form of time-averaged R^* in [32] while the increase in heat transfer due to internal circulation can be modelled by introducing an enhanced liquid thermal conductivity of the form

$$k_L^{*\prime} = k_L^* (1 + \beta \, \mathrm{Re}_L^{1/2} \mathrm{Pr}_L^{1/3}), \quad [34]$$

where β is a constant and the familiar last term accounts for the convective contribution. Since the intensity of internal circulation depends on the external flow, the continuity of tangential shear stress at the droplet surface can be used to relate Re_L to Re_∞:

$$\frac{\mu_L^* v_s^*}{\delta_L^*} \approx \frac{\mu_G^* v_\infty^*}{\delta_G^*}. \quad [35]$$

It is well-known from laminar boundary-layer theory that

$$\delta^* \approx \frac{R^*}{\mathrm{Re}^{1/2}}. \quad [36]$$

Hence, using [35] and [36], Re_L is related to Re_∞ as

$$\mathrm{Re}_L^{1/2} \approx \mathrm{Re}_\infty^{1/2} \left(\frac{\rho_L^*}{\rho_\infty^*}\right)^{1/3} \left(\frac{\mu_\infty^*}{\mu_L^*}\right)^{2/3}. \quad [37]$$

In the model, [37] is treated as a formal equality, and the departure from this is absorbed by β.

Finally, the complete set of equations in non-dimensional form are

$$\frac{\mathrm{d}\left(\frac{m}{m_0}\right)}{\mathrm{d}t} = -\frac{3\mathrm{Nu}_\infty B'_\infty R}{\mathrm{Re}_0 \mathrm{Pr}_\infty \rho_{L,0}} \quad [38]$$

and

$$\frac{\mathrm{d}V}{\mathrm{d}t} = -\frac{3C_D R^2 V^2}{8\rho_{L,0}\left(\frac{m}{m_0}\right)}, \quad [39]$$

where

$$R = \left[\left(\frac{m}{m_0}\right)\left(\frac{\rho_{L,0}}{\rho_L}\right)\right]^{1/3}, \tag{40}$$

$$B' = B\left(1 - \frac{Q_L}{Q_G}\right), \tag{41}$$

$$\frac{Q_L}{Q_G} = \frac{4Rk'_L(T_s - T_0)}{Nu_\infty(1 - T_s)} \sum_{j=1}^{\infty} \frac{1}{\tilde{R}} \exp\left(\frac{-2\pi^2 j^2 \tilde{k}'_L t}{Re_0 Pr_\infty \tilde{R}^2 \rho_L c_{p,L}}\right), \tag{42}$$

$$Nu_\infty = k_f(1 + B'_f)^{-0.7}(2 + 0.57\, Re_m^{1/2} Pr_f^{1/3}), \tag{43}$$

$$C_D = (1 + B'_f)^{-0.2}(24\, Re_m^{-1} + 4.8\, Re_m^{-0.37}), \tag{44}$$

$$k'_L = k_L\left[1 + 0.056\, Pr_L^{1/3}\, \mu_f^{1/2}\left(\frac{\rho_L}{\mu_L^2}\right)^{1/3} Re_m^{1/2}\right] \tag{45}$$

and

$$Re_\infty = \mu_f Re_m = VR\, Re_0. \tag{46}$$

Here, [28] and [30] were combined to yield [38], and [39] is the non-dimensional form of [29]. Equations [43] and [44] are the previously given Renksizbulut–Yuen correlations, and [34] and [37] were combined to obtain [45] where $\beta = 0.056$ has been used, the reason for which will be given in the next section. Equation [42] follows from [32] and [33] where the time averaging is over the last n time steps, i.e.

$$\frac{1}{\tilde{R}} = \frac{1}{n}\sum_{i=1}^{n}\frac{1}{R_i}, \quad \frac{1}{\tilde{R}^2} = \frac{1}{n}\sum_{i=1}^{n}\frac{1}{R_i^2}, \quad \tilde{k}'_L = \frac{1}{n}\sum_{i=1}^{n}\tilde{k}'_{L,i}. \tag{47}$$

The initial conditions are simply $m/m_0 = 1$ and $V = 1$.

Because of the strong coupling between these equations, an iterative procedure is required at each time step in order to arrive at the correct Q_L/Q_G ratio. The solution algorithm is as follows:

1. Start a new time step by guessing Q_L/Q_G.
2. Calculate B' and then Nu_∞ and C_D.
3. Calculate m/m_0, V and R at the new time step from [38]–[40].
4. Calculate Q_L/Q_G from [42].
5. Return to step 2 if Q_L/Q_G has changed by more than a prescribed percentage (such as 0.1%). Otherwise, move on to the next time plane by returning to step 1.

7. RESULTS OF THE SEMI-ANALYTICAL MODEL

The predictive capability of the semi-analytical model was evaluated using the results obtained from the fully numerical analysis presented before. In the model calculations, all liquid thermophysical properties were evaluated at the arithmetic mean temperature based on the initial and saturation temperatures. At this mean temperature $Pr_L = 6.01$, $Re_L = 1.266\, Re_\infty$ and $Pr_L = 5.31$, $Re_L = 0.437\, Re_\infty$ for the low- and high-pressure cases, respectively. Thus, the liquid-phase Péclet numbers (RePr) varied from about 760 to 50 during the droplet lifetimes.

Shown in figures 10–12 are the mass, liquid heating, Reynolds number, drag coefficient and Nusselt number histories for the low-pressure case. The observed agreement is remarkable in view of the overwhelming simplicity of the model as compared to the fully numerical scheme. It should be noted that $\beta = 0.056$ appearing in [45] for k'_L was obtained using the low-pressure numerical data on Q_L/Q_G as reference. However, with this final calibration, [45] should be applicable to other cases like any other correlation.

The predictions of the simple model for the high-pressure case are shown in figures 13–16. Although the agreement now is not as good as the low-pressure case, the results are still within 20% of the fully numerical predictions on droplet mass, Reynolds number, drag coefficient and Nusselt number. This reduction in predictive capability with increasing pressure is primarily due

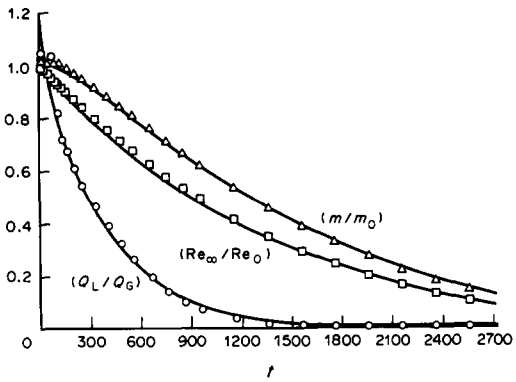

Figure 10. Comparison of the model predictions (——) with the numerical solutions (△, □, ○) at 1 bar; $Re_0 = 100$.

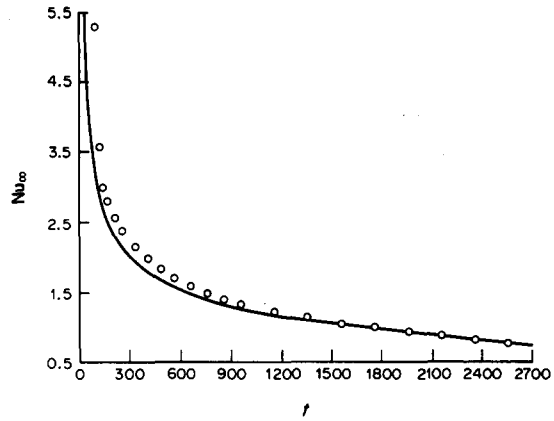

Figure 11. Comparison of the model predictions (——) with the numerical solution (○) for the Nusselt number history at 1 bar; $Re_0 = 100$.

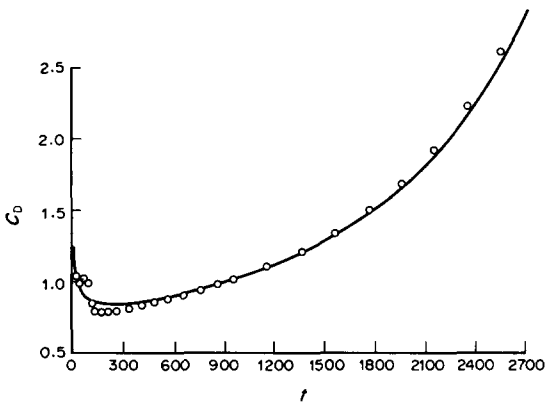

Figure 12. Comparison of the model predictions (——) with the numerical solution (○) for the drag coefficient at 1 bar; $Re_0 = 100$.

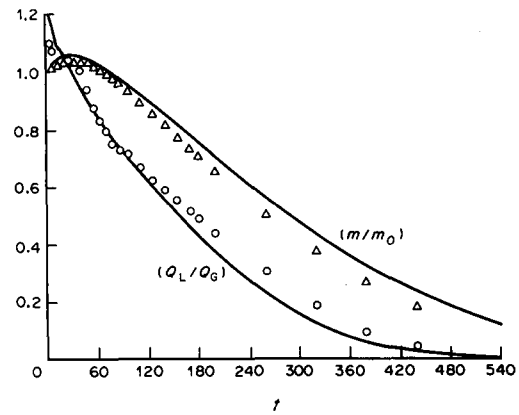

Figure 13. Comparison of the model predictions (——) with the numerical solutions (△, ○) at 10 bar; $Re_0 = 250$.

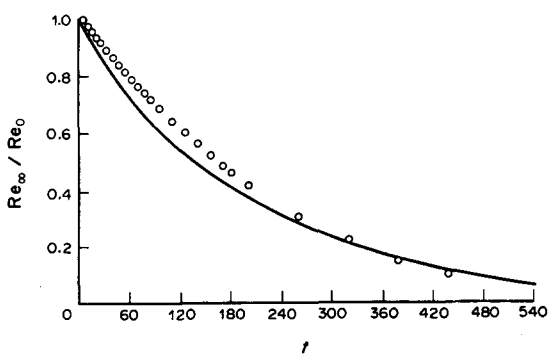

Figure 14. Comparison of the model predictions (——) with the numerical solution (○) for the Reynolds number history at 10 bar; $Re_0 = 250$.

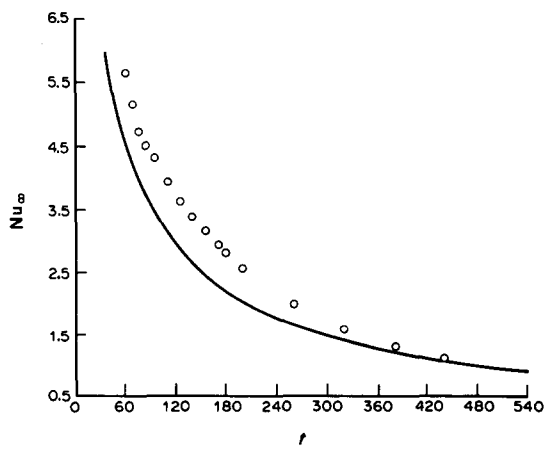

Figure 15. Comparison of the model predictions (——) with the numerical solution (○) for the Nusselt number history at 10 bar; $Re_0 = 250$.

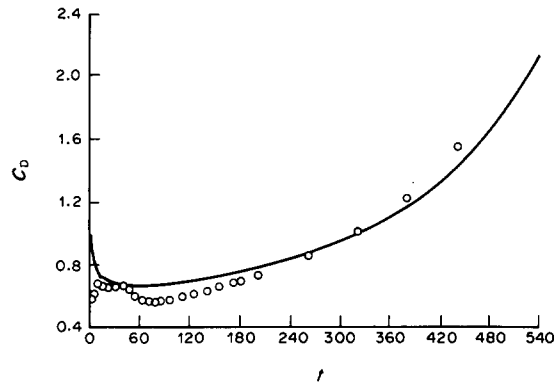

Figure 16. Comparison of the model predictions (——) with the numerical solution (○) for the drag coefficient at 10 bar; $Re_0 = 250$.

to increased surface mobility and stronger gas-phase transient effects which are difficult to model with existing Nusselt number and drag correlations in a quasi-steady manner, as discussed previously in section 5.

Finally, it should be noted that a very similar procedure can be followed when the droplet is evaporating in a medium other than its own vapour as more commonly encountered in practice. In such a case, a Sherwood number correlation is needed as an additional equation because the droplet surface temperature T_s is now an additional unknown. The iterative process then involves seeking the correct T_s as well as Q_L which would satisfy [3] at a given time.

8. CONCLUSION

This research was motivated by spray modelling studies that require accurate correlations for droplet drag and heat transfer as fundamental inputs. As such, the principal conclusion of the present work, based on a complete numerical study of transient convective evaporation of *n*-heptane droplets at 1 and 10 bar, is that the Renksizbulut–Yuen correlations together with an enhanced diffusion model for liquid-phase heating can be used in a quasi-steady manner to predict droplet behaviour quite accurately. However, more research is needed before this conclusion can be safely extended to the pressures well above 10 bar encountered in some spray applications.

Acknowledgements—This work is supported by an operating grant from the Natural Sciences and Engineering Research Council of Canada to M. Renksizbulut, and by a graduate student scholarship from the Ontario Government to R. Haywood.

NOMENCLATURE

B = Transfer number, $(T^*_\infty - T^*_s)\, c^*_{p,G}/L^*$
c_p = Specific heat at constant pressure, $c^*_p/c^*_{p\infty}$
C_D = Total drag coefficient, $2F^*/\rho^*_\infty v^{*2}_\infty \pi R^{*2}$
F^* = Total force acting on the droplet
h^* = Heat transfer coefficient
k = Thermal conductivity, k^*/k^*_∞
L = Latent heat of vaporization, $L^*/c^*_{p\infty} T^*_\infty$
$\dot{m}''_\theta$ = Local mass flux, $\dot{m}''^*_\theta/\rho^*_\infty v^*_{\infty,0}$
Nu = Nusselt number, $2R^*h^*/k^*$
p = Pressure, $(p^* - p^*_\infty)/\rho^*_\infty v^{*2}_{\infty,0}$
Pr = Prandtl number, $\mu^* c^*_p/k^*$
Q^* = Heat transfer rate
r = Radial coordinate, r^*/R^*
R = Instantaneous droplet size, R^*/R^*_0

R_0^* = Initial droplet size
Re = Reynolds number, $2R^*\rho^*v^*/\mu^*$
Re_0 = Initial Reynolds number, $2R_0^*\rho_\infty^*v_{\infty,0}^*/\mu_\infty^*$
Re_m = Reynolds number, $2R^*\rho_\infty^*v_\infty^*/\mu_f^*$
t = Time, $t^*v_{\infty,0}^*/R_0^*$
T = Temperature, T^*/T_∞^*
v_∞^* = Instantaneous free-stream velocity
v_r = Radial velocity, v_r^*/v_∞^*
v_θ = Tangential velocity, v_θ^*/v_∞^*
V = Instantaneous free-stream velocity, $v_\infty^*/v_{\infty,0}^*$
We = Weber number, $2R^*\rho_\infty^*v_\infty^{*2}/\sigma^*$

Greek symbols

α^* = Thermal diffusivity, $k^*/\rho^*c_p^*$
δ = Boundary-layer thickness, δ^*/R^*
θ = Tangential coordinate
μ = Viscosity, μ^*/μ_∞^*
ν^* = Kinematic viscosity, μ^*/ρ^*
ρ = Density, ρ^*/ρ_∞^*
σ^* = Surface tension
$\tau_{r\theta}^*$ = Shear stress
τ_{rr}^* = Normal stress

Subscripts and superscripts

f = Film condition
G = Gas phase
L = Liquid phase
0 = Initial conditions
s = At the droplet surface
sat = Saturation conditions
∞ = Free-stream conditions
* = Dimensional quantity
$\hat{}$ = Unit vector
$\bar{}$ = Spatial average

REFERENCES

CARSLAW, H. S. & JAEGER, J. C. 1959 *Conduction of Heat in Solids*, 2nd edn, p. 233. OUP, Oxford.

DWYER, H. A. & SANDERS, B. R. 1984a Detailed computation of unsteady droplet dynamics. In *Proc. 20th Symp. (Int.) on Combustion*, The Combustion Institute, Pittsburgh, Pa, pp. 1743–1749.

DWYER, H. A. & SANDERS, B. R. 1984b Droplet dynamics and vaporization with pressure as a parameter. Presented at *ASME Winter A. Mtg*, New Orleans, La.

FAETH, G. M. 1977 Current status of droplet and liquid combustion. *Prog. Energy Combust. Sci.* **3,** 191–224.

FAETH, G. M. 1983 Evaporation and combustion of sprays. *Prog. Energy Combust. Sci.* **9,** 1–76.

FENDELL, F. E., SPRANKLE, M. L. & DODSON, D. S. 1966 Thin flame theory for a fuel drop in slow viscous flow. *J. Fluid Mech.* **26,** 267–280.

GAL-OR, B. & YARON, I. 1973. Diffusion drag upon slowly evaporating drops. *Phys. Fluids* **16,** 1826–1829.

GODSAVE, G. A. E. 1953 Studies of the combustion of drops in a fuel spray: the burning of single drops of fuel. In *Proc. 4th Symp. (Int.) on Combustion*, The Combustion Institute, Pittsburgh, Pa, pp. 818–830.

GOGOS, G., SADHAL, S. S., AYYASWAMY, P. S. & SUNDARARAJAN, T. 1986 Thin-flame theory for the combustion of a moving liquid drop: effects due to variable density. *J. Fluid Mech.* **171,** 121–144.

HAYWOOD, R. 1986 Variable-property, blowing and transient effects in convective droplet evaporation with internal circulation. M.A.Sc. Thesis, Univ. of Waterloo, Ontario.

HAYWOOD, R. & RENKSIZBULUT, M. 1986 On variable-property, blowing, and transient effects in convective droplet evaporation with internal circulation. In *Proc. 8th Int. Heat Transfer Conf.*, San Francisco, Calif., Vol. 4, pp. 1861–1866.

LARA-URBANEJA, P. & SIRIGNANO, W. A. 1981 Theory of transient multicomponent droplet vaporization in a convective field. In *Proc. 18th Symp. (Int.) on Combustion*, The Combustion Institute, Pittsburgh, Pa, pp. 1365–1374.

LAW, C. K. 1983 Recent advances in droplet vaporization and combustion. *Prog. Energy Combust. Sci.* **8,** 171–201.

MONTLUCON, J. 1975 Heat and mass transfer in the vicinity of an evaporating droplet. *Int. J. Multiphase Flow* **2,** 171–182.

PATANKAR, S. V. 1980 *Numerical Heat Transfer and Fluid Flow*, p. 113. McGraw-Hill, New York.

PRAKASH, S. & SIRIGNANO, W. A. 1980 Theory of convective droplet vaporization with unsteady heat transfer in the circulating liquid phase. *Int. J. Heat Transfer* **23,** 253–268.

RENKSIZBULUT, M. & YUEN, M. C. 1983a Numerical study of droplet evaporation in a high temperature stream. *J. Heat Transfer* **105,** 389–397.

RENKSIZBULUT, M. & YUEN, M. C. 1983b Experimental study of droplet evaporation in a high temperature air stream. *J. Heat Transfer* **105,** 384–388.

SADHAL, S. S. & AYYASWAMY, P. S. 1983 Flow past a liquid drop with a large non-uniform radial velocity. *J. Fluid Mech.* **133,** 65–81.

SIRIGNANO, W. A. 1983 Fuel droplet vaporization and spray combustion theory. *Prog. Energy Combust. Sci.* **9,** 291–322.

SPALDING, D. B. 1953 The combustion of liquid fuels. In *Proc. 4th Symp. (Int.) on Combustion*, The Combustion Institute, Pittsburgh, Pa, pp. 847–864.

TAYLOR, T. D. & ACRIVOS, A. 1964 On the deformation and drag of a falling viscous drop at low Reynolds numbers. *J. Fluid Mech.* **18,** 466–476.

VANDOORMAAL, J. P. & RAITHBY, G. D. 1984 Enhancements of the SIMPLEC method for predicting incompressible fluid flows. *Numer. Heat Transfer* **7,** 147–163.

WILLIAMS, A. 1973 Combustion of droplets of liquid fuels: a review. *Combust. Flame* **21,** 1–31.

WILLIAMS, F. A. 1985 *Combustion Theory*, 2nd edn, p. 448. Benjamin Cummings, Menlo Park, Calif.